A Nonlinear Delay-Differential Equation with Harmonic Excitation

János Lelkes * **, Tamás Kalmár-Nagy** *

* *Department of Fluid Mechanics, Faculty of Mechanical Engineering, Budapest University of Technology and Economics, Budapest 1111, Hungary (e-mail: jani1234321@gmail.com, ifac2018@kalmarnagy.com).*

Abstract: A machining tool can be subject to different kinds of excitations. The forcing may have external sources (such as rotating imbalance or misalignment of the workpiece) or it can arise from the cutting process itself (e.g. chip formation). We investigate the classical tool vibration model which is a delay-differential equation with a quadratic and cubic nonlinearity and periodic forcing. The method of multiple scales gave an excellent approximation of the solution. The resonance curves found here are similar to those for the Duffing-equation, having a hardening characteristic. We found subcritical Hopf and saddle-node bifurcations.

Keywords: delay-differential equation, method of multiple scales, harmonic excitation, Hopf bifurcation, primary resonance

1. INTRODUCTION

Delay-differential equations (DDEs) are important in many areas of engineering and science. For example in stability analysis, computational techniques (symbolic and numerical), automotive engineering, manufacturing, neuroscience, and control theory (see Balachandran et al. [2009]).

In this paper the nondimensional form of a regenerative one-degree-of-freedom machine tool vibration model in the case of orthogonal cutting is investigated (for derivation see Kalmár-Nagy et al. [2001])

$$\ddot{x} + 2\zeta\dot{x} + x = p\left(x_\tau - x\right) + q\left(\left(x - x_\tau\right)^2 - \left(x - x_\tau\right)^3\right) + A\cos\left(\omega t\right), \tag{1}$$

where x is the tool displacement ($x_\tau = x\left(t-\tau\right)$ is its delayed value with delay $\tau > 0$), $\zeta > 0$ is the relative damping factor, $p > 0$ is the nondimensional cutting force, $q > 0$ is the coefficient of nonlinearity, A is the amplitude of the forcing and ω is its frequency.

Perturbation methods were successfully applied to delay-differential equations (such as the Linstedt-Poincaré method (Casal and Freedman [1980]), the method of multiple scales (Nayfeh et al. [1997], Nayfeh [2008], Oztepe et al. [2015]) or the combination of the method of multiple scales and Linstedt-Poincaré method (Pakdemirli and Karahan [2010]).

We will approximate the solution by using the method of multiple scales. In the following we will assume that damping is small, the nonlinearity and forcing are weak (see Kalmár-Nagy [2002]). In particular

$$\zeta,\, p,\, q,\, A \sim O\left(\varepsilon\right), \qquad \omega = 1 + \varepsilon\sigma, \tag{2}$$

where $\varepsilon \ll 1$ and σ is the detuning frequency. We also assume that the solution of (1) can be well approximated by the two-scale expansion

$$x\left(t\right) = x_0\left(t_0, t_1\right) + \varepsilon x_1\left(t_0, t_1\right) + O\left(\varepsilon^2\right), \tag{3}$$

where the timescales are defined as

$$t_0 = t, \quad t_1 = \varepsilon t. \tag{4}$$

With the differential operators

$$D_0 = \frac{\partial}{\partial t_0}, \quad D_1 = \frac{\partial}{\partial t_1}, \tag{5}$$

time differentiation can be written as

$$\frac{d}{dt} = D_0 + \varepsilon D_1 + O\left(\varepsilon^2\right), \tag{6}$$

and similarly

$$\frac{d^2}{dt^2} = D_0^2 + 2\varepsilon D_0 D_1 + O\left(\varepsilon^2\right). \tag{7}$$

2. LINEAR STABILITY ANALYSIS OF THE UNFORCED SYSTEM

The stability analysis of the $x = 0$ solution of the linearized equation

$$\ddot{x} + 2\zeta\dot{x} + x = p\left(x_\tau - x\right), \tag{8}$$

was performed in, for example, Hanna and Tobias [1974], Stépán [1989]. The stability boundaries of (8) is obtained by substituting the trial solution $x(t) = C\exp(i\Omega t)$ into (8). The stability diagram in Figure 1 is given in parametric form in Kalmár-Nagy [2002] as

$$p = \frac{\left(1-\Omega^2\right)^2 + 4\zeta^2\Omega^2}{2\left(\Omega^2 - 1\right)}, \tag{9}$$

$$\tau = \frac{2}{\Omega}\left(j\pi - \arctan\frac{\Omega^2 - 1}{2\zeta\Omega}\right), \quad j = 1, 2, \ldots, \tag{10}$$

where j corresponds to the jth 'lobe' and $\Omega > 1$ because $p > 0$.

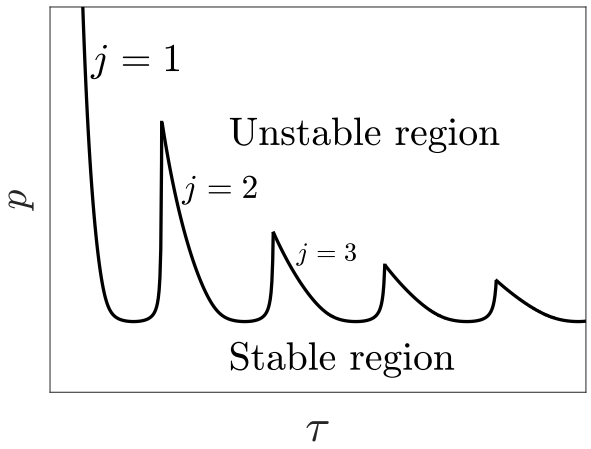

Fig. 1. The linear stability chart of (1)

At the minima ('notches') of the stability lobes, Ω, p, τ assume the particularly simple forms

$$\Omega_{crit} = \sqrt{1+2\zeta}, \tag{11}$$

$$p_{crit} = 2\zeta\left(\zeta+1\right), \tag{12}$$

$$\tau_{crit} = \frac{2\left(j\pi - \arctan\frac{1}{\sqrt{1+2\zeta}}\right)}{\sqrt{1+2\zeta}}, \quad j = 1,2,\ldots \tag{13}$$

3. THE LINEAR DELAY-DIFFERENTIAL EQUATION WITH HARMONIC FORCING

Here we study the harmonically forced linear equation

$$\ddot{x} + 2\zeta\dot{x} + x = p\left(x_\tau - x\right) + A\cos\left(\omega t\right). \tag{14}$$

With assumption (2), substituting the differential operators (6) and (7) into (14) and equating like powers of ε one obtains

$$\varepsilon^0: \quad D_0^2 x_0\left(t_0,t_1\right) + x_0\left(t_0,t_1\right) = 0, \tag{15}$$

$$\begin{aligned}\varepsilon^1: \quad & D_0^2 x_1\left(t_0,t_1\right) + x_1\left(t_0,t_1\right) = -2D_0D_1x_0\left(t_0,t_1\right)\\ & -2\zeta D_0 x_0\left(t_0,t_1\right) + p\left[x_0\left(t_0-\tau,t_1\right) - x_0\left(t_0,t_1\right)\right]\\ & +A\cos\left(t_0+\sigma t_1\right).\end{aligned} \tag{16}$$

Solving (15) for $x_0\left(t_0,t_1\right)$, knowing that the slow temporal variable t_1 is implicit in the constants of integration, we get

$$x_0\left(t_0,t_1\right) = a\left(t_1\right)e^{it_0} + \bar{a}\left(t_1\right)e^{-it_0}, \tag{17}$$

We substitute this solution into (16) and eliminate the secular terms which would give rise to unbounded terms

$$0 = -\frac{1}{2}Ae^{i\sigma t_1} + 2iD_1a\left(t_1\right) + a\left(t_1\right)\left[p - e^{-i\tau}p + 2i\zeta\right]. \tag{18}$$

Writing $a\left(t_1\right)$ in a polar form (where $\alpha\left(t_1\right)$ is the amplitude and $\beta\left(t_1\right)$ is the phase)

$$a\left(t_1\right) = \frac{1}{2}\alpha\left(t_1\right)e^{i\beta(t_1)}, \qquad \bar{a}\left(t_1\right) = \frac{1}{2}\alpha\left(t_1\right)e^{-i\beta(t_1)}, \tag{19}$$

then substituting into (18), we get

$$\begin{aligned}0 = & -\frac{1}{2}Ae^{i\sigma t_1} + i\left(D_1\alpha\left(t_1\right) + i\alpha\left(t_1\right)D_1\beta\left(t_1\right)\right)e^{i\beta(t_1)}\\ & +\frac{1}{2}\alpha\left(t_1\right)e^{i\beta(t_1)}\left[p - e^{-i\tau}p + 2i\zeta\right].\end{aligned} \tag{20}$$

Now we divide (20) by $e^{i\beta(t_1)}$ and introduce

$$\phi\left(t_1\right) = \sigma t_1 - \beta\left(t_1\right), \tag{21}$$

to get

$$\begin{aligned}0 = & -\frac{1}{2}Ae^{i\phi(t_1)} + i\left(D_1\alpha\left(t_1\right) + i\left(\sigma - D_1\phi(t_1)\right)\right)\\ & +\frac{1}{2}\alpha\left(t_1\right)\left[p - e^{-i\tau}p + 2i\zeta\right].\end{aligned} \tag{22}$$

Separating the real and imaginary parts of equation (22) results in two ordinary differential equations describing the evolution of the amplitude and phase

$$D_1\alpha = -\left(\zeta + \frac{p}{2}\sin\tau\right)\alpha + \frac{A}{2}\sin\phi, \tag{23}$$

$$\alpha D_1\phi = \frac{1}{2}\left(p\cos\tau + 2\sigma - p\right)\alpha + \frac{A}{2}\cos\phi. \tag{24}$$

To get the amplitude and phase of the steady-state primary resonance (i.e. the fixed point of (23) and (24)) we set the left-hand sides of (23) and (24) to zero and solve the resulting algebraic equations (by eliminating the trigonometric terms from them). For the amplitude α^* and phase ϕ^* we get

$$\alpha^* = \frac{A}{\sqrt{\left(p\left(1-\cos\tau\right) - 2(\omega-1)\right)^2 + 4\left(\zeta + \frac{p}{2}\sin\tau\right)^2}}. \tag{25}$$

$$\phi^* = \arcsin\left(2\left(\zeta + \frac{p}{2}\sin\tau\right)\frac{\alpha}{A}\right). \tag{26}$$

The stability of the fixed point (α^*, ϕ^*) is determined by the Jacobian

$$\boldsymbol{J} = \begin{pmatrix} -\zeta - \frac{p}{2}\sin\tau & \frac{A}{2}\cos\phi^* \\ -\frac{A}{2\alpha^{*2}}\cos\phi^* & -\frac{A}{2\alpha}\sin\phi^* \end{pmatrix}. \tag{27}$$

The trace and determinant of $\boldsymbol{J}$ are

$$T = -2\zeta - p\sin\tau, \tag{28}$$

$$\Delta = \left(\zeta + \frac{p}{2}\sin\tau\right)^2 + \frac{1}{4}(p(1-\cos\tau) - 2\omega + 2)^2. \tag{29}$$

The determinant Δ is always non-negative. The discriminant

$$T^2 - 4\Delta = -(p(1-\cos\tau) - 2\omega + 2)^2 \le 0, \tag{30}$$

therefore the fixed point is a stable spiral when $T < 0$, a center when $T = 0$ (at $p_{bif} = -2\frac{\zeta}{\sin\tau}$), and an unstable spiral when $T > 0$.

We chose p as the bifurcation parameter. The phase portraits of the "slow-flow" (Eqs. (23) and (24)) are shown in Figs. 2, 3, 4 for different p values.

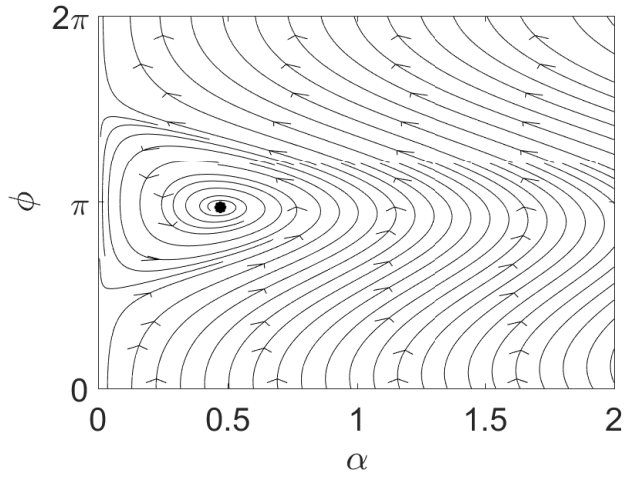

Fig. 2. Stable spiral $p < p_{bif}$

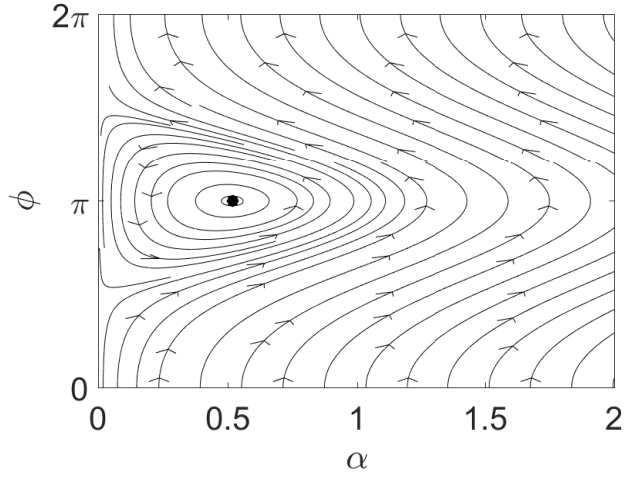

Fig. 3. Center $p = p_{bif}$

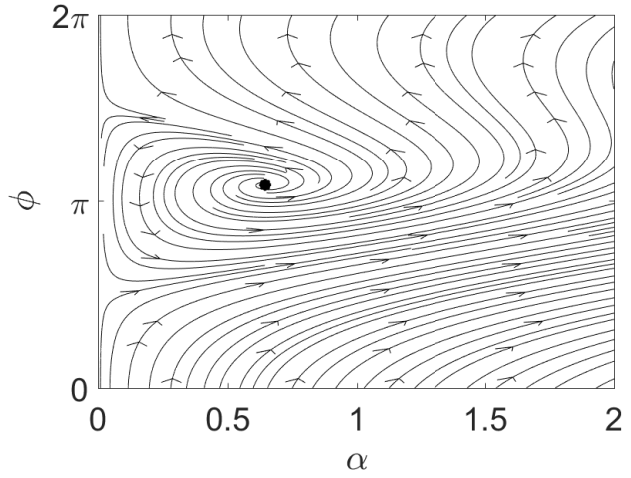

Fig. 4. Unstable spiral $p > p_{bif}$

3.1 Numerical results

The direct numerical solution of (14) was determined in Mathematica using the Dormand-Prince method with an initial function $\alpha^* \cos(\omega t + \phi^*)$, $t \in [-\tau, 0]$, where α^* and ϕ^* were determined from (25) and (26). The following numerical values were chosen for the simulation

$$\zeta = 0.01, \quad A = 0.01. \tag{31}$$

We have chosen p values at the first 'notch' ($j = 1$). Using (12) and (13) gives

$$p_{crit} = 0.0202, \quad \tau_{crit} = 4.676. \tag{32}$$

Time series $x(t)$ for

$$p = \{0.75p_{crit}, 0.90p_{crit}, 0.99p_{crit}, 1.05p_{crit}\} \tag{33}$$

are shown in Figure 5.

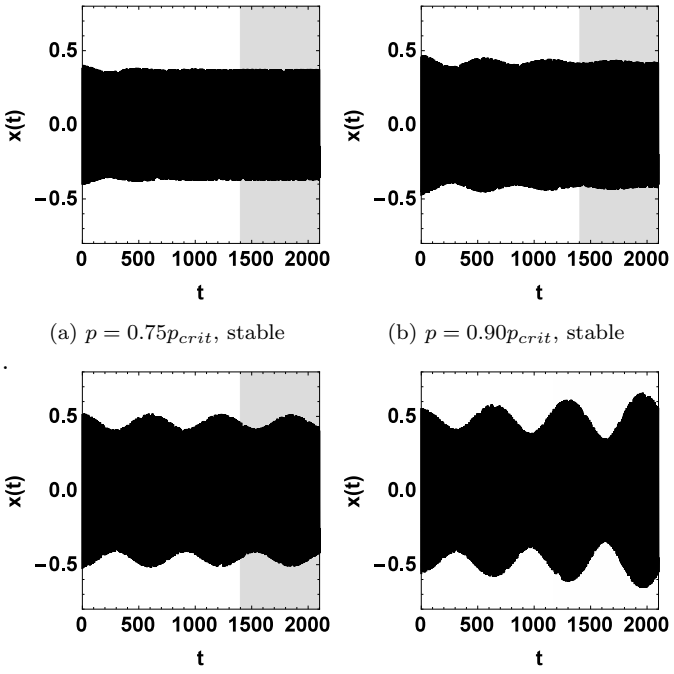

(a) $p = 0.75p_{crit}$, stable (b) $p = 0.90p_{crit}$, stable

(c) $p = 0.99p_{crit}$, stable (d) $p = 1.05p_{crit}$, unstable

Fig. 5. Time series of the numerical solution ($\omega = 1.02$)

The grey areas indicate the time interval $[300\tau, 450\tau]$ where the steady state vibration amplitude of the numerical solution was determined as

$$\alpha_{num} = \max|x(t)|, \quad t \in [300\tau, 450\tau]. \tag{34}$$

In the case of $p = 0.90p_{crit}$ and $p = 0.99p_{crit}$ the vibration becomes modulated, so the amplitude of the vibration also varies between a certain range during the simulation. For a better comparison of the method of multiple scales and numerical results we introduce the method of multiple scales amplification factor G^* and numerical amplification factor G_{num} as

$$G^* := \frac{\alpha^*}{A}, \quad G_{num} := \frac{\alpha_{num}}{A}. \tag{35}$$

The comparison of the amplification factors G^* and G_{num} is shown in Figure 6, where the solid line indicates the method of multiple scales (MMS) results, the dots the numerical results.

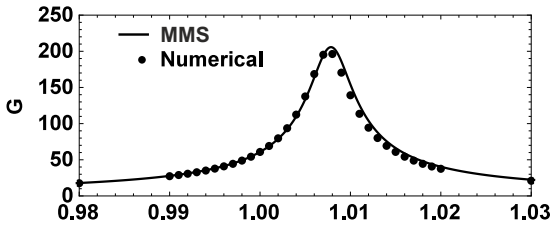

(a) $p = 0.75p_{crit}$

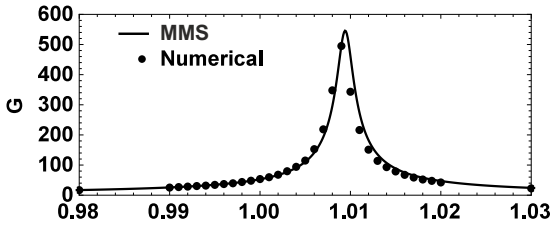

(b) $p = 0.90p_{crit}$

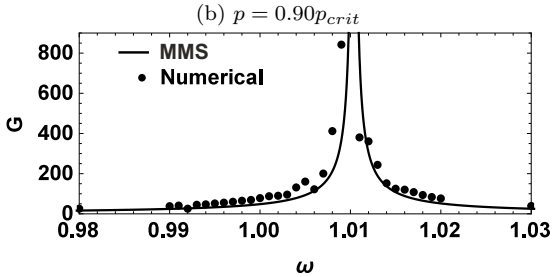

(c) $p = 0.99p_{crit}$

Fig. 6. The amplification factor G as a function of ω

4. THE HARMONICALLY FORCED NONLINEAR DELAY-DIFFERENTIAL EQUATION

Substituting the differential operators (6) and (7) into (1) and equating like powers of ε one obtains

$$\varepsilon^0: \quad D_0^2 x_0(t_0,t_1) + x_0(t_0,t_1) = 0, \tag{36}$$

$$\begin{aligned}\varepsilon^1: \quad & D_0^2 x_1(t_0,t_1) + x_1(t_0,t_1) = -2D_0D_1x_0(t_0,t_1) \\ & -2\zeta D_0 x_0(t_0,t_1) + p\left[x_0(t_0-\tau,t_1) - x_0(t_0,t_1)\right] \\ & +q\left[x_0(t_0-\tau,t_1) - x_0(t_0,t_1)\right]^2 \\ & +q\left[x_0(t_0-\tau,t_1) - x_0(t_0,t_1)\right]^3 + A\cos(t_0+\sigma t_1).\end{aligned} \tag{37}$$

Solving (36) for $x_0(t_0,t_1)$ yields

$$x_0(t_0,t_1) = a(t_1)e^{it_0} + \bar{a}(t_1)e^{-it_0}. \tag{38}$$

Then we substitute this solution into (37) and eliminate the secular terms which would give rise to unbounded terms

$$\begin{aligned}0 = & -\frac{1}{2}Ae^{i\sigma t_1} + 2iD_1a(t_1) \\ & +a(t_1)\left[p - e^{-i\tau}p + 2i\zeta - 3e^{-2i\tau}\left(e^{i\tau}-1\right)^3 qa(t_1)\bar{a}(t_1)\right].\end{aligned} \tag{39}$$

Writing $a(t_1)$ in a polar form (where $\alpha(t_1)$ is the amplitude and $\beta(t_1)$ is the phase)

$$a(t_1) = \frac{1}{2}\alpha(t_1)e^{i\beta(t_1),} \qquad \bar{a}(t_1) = \frac{1}{2}\alpha(t_1)e^{-i\beta(t_1)\cdot} \tag{40}$$

then substituting into (39) using (21) and separating the real and imaginary parts results in two ordinary differential equations describing the evolution of the amplitude and phase

$$D_1\alpha = -\left(\zeta + \frac{p}{2}\sin\tau\right)\alpha - 3q\cos\frac{\tau}{2}\sin^3\frac{\tau}{2}\alpha^3 + \frac{A}{2}\sin\phi, \tag{41}$$

$$\alpha D_1\phi = \frac{1}{2}\left(p\cos\tau + 2\sigma - p\right)\alpha - 3q\sin^4\frac{\tau}{2}\alpha^3 + \frac{A}{2}\cos\phi. \tag{42}$$

To get the amplitude of the steady-state primary resonance i.e. the fixed points of (41) and (42) we set the left-hand sides of (41) and (42) to zero and solve the resulting algebraic equations (by eliminating the trigonometric terms from them)

$$\begin{aligned}&\left[\frac{1}{4}\left(p(1-\cos\tau) - 2\sigma + 6q\alpha^{*2}\sin^4\frac{\tau}{2}\right)^2\right. \\ &\left.+\left(\zeta + \frac{p}{2}\sin\tau + 3q\alpha^{*2}\cos\frac{\tau}{2}\sin^3\frac{\tau}{2}\right)^2\right]\alpha^{*2} - \frac{A^2}{4} = 0.\end{aligned} \tag{43}$$

$$\phi^* = \arcsin\left(\frac{2}{A}\left(\zeta + \frac{p}{2}\sin\tau\right)\alpha^* + 3q\cos\frac{\tau}{2}\sin^3\frac{\tau}{2}\alpha^{*3}\right). \tag{44}$$

Equation (43) can be solved for α^* resulting $1, 2$ or 3 pair $(\pm)$ of real roots.

Stability of the fixed points (α^*, ϕ^*) is determined by the Jacobian

$$\boldsymbol{J} = \begin{pmatrix} -\zeta - \frac{p}{2}\sin\tau - 9q\alpha^{*2}\cos\frac{\tau}{2}\sin^3\frac{\tau}{2} & \frac{A}{2}\cos\phi^* \\ -6\alpha^* q\sin^4\frac{\tau}{2} - \frac{A}{2\alpha^{*2}}\cos\phi^* & -\frac{A}{2\alpha^*}\sin\phi^* \end{pmatrix}. \tag{45}$$

The stability of the fixed points can be investigated by calculating the determinant Δ, the trace T and the discriminant $T^2 - 4\Delta$ of $\boldsymbol{J}$.

The nondimensional cutting force coefficient was taken to be $p = 0.5p_{crit}$, the coefficient of nonlinearity $q = 0.003$, forcing amplitude $A = 0.01$. The quantity ω was chosen as bifurcation parameter, increased from 0.98 to 1.03.

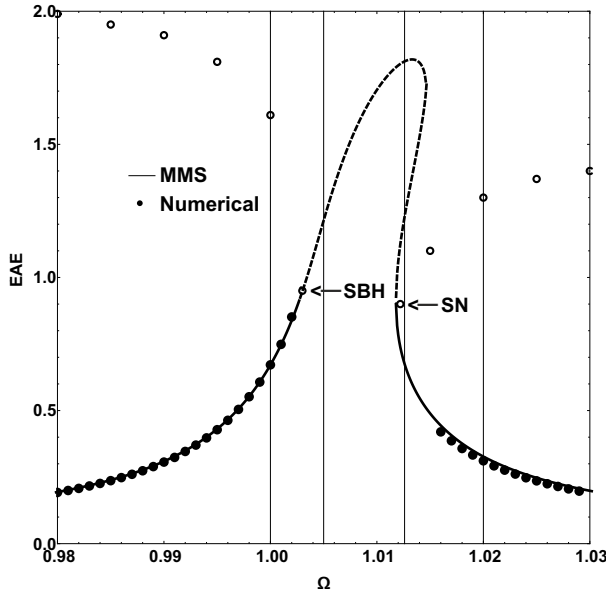

Fig. 7. Bifurcation diagram (or resonance curve), where SBH corresponds to subcritical Hopf bifurcation and SN to saddle-node bifurcation.

Figure 7 shows the amplitude α^* as a function of forcing frequency ω (the solid line indicates stable solution, the dashed line the unstable solution, both method of multiple scales solution). The stable numerical equlibrium solutions are shown with filled circles, unstable limit cycles are depicted by empty circles. The thin vertical lines in Fig. 7 indicate the ω values $(1.00,\ 1.005, 1.013, 1.02)$ for which the phase portraits of Figs. (8-11) were generated.

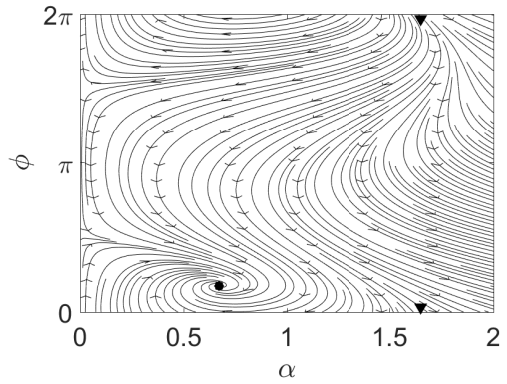

Fig. 8. Stable spiral at $\omega = 1$, the arrowheads indicate two points of the unstable limit cycle

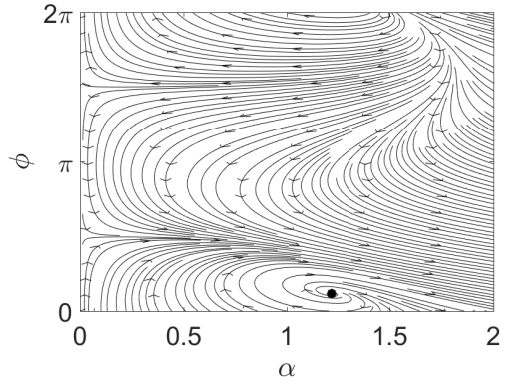

Fig. 9. Unstable spiral at $\omega = 1.005$

Subcritical Hopf bifurcation occurs at $\omega \approx 1.003$, see Figure 8 and 9.

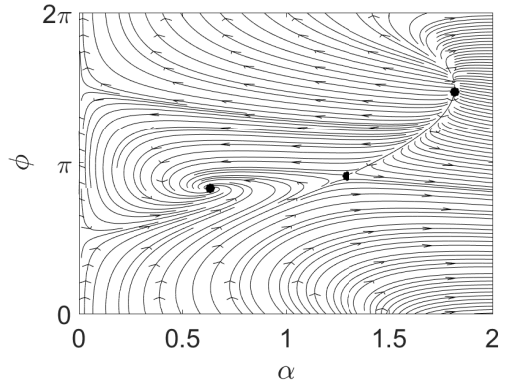

Fig. 10. Stable spiral at $\omega = 1.013$ and two unstable fixed points

A saddle and a node connected with a heteroclinic orbit can be observed at $\omega \approx 1.013$, see Figure 10.

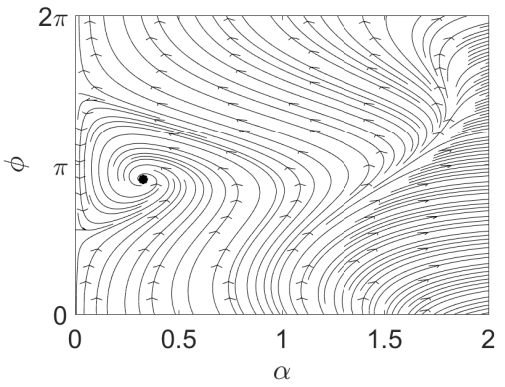

Fig. 11. Stable spiral and unstable limit cycle at $\omega = 1.02$

5. CONCLUSIONS

The method of multiple scales gave an excellent approximation of the solution of the nonlinear delay-differential equation (1). The resonance curves found here are similar to those for the Duffing-equation (Nayfeh and Mook [1979]), having a hardening characteristic. We found subcritical Hopf bifurcations and saddle-node bifurcations.

Equation (1) without forcing admits a subcritical Hopf bifurcation (Kalmár-Nagy [2002]) and the interaction of forcing and Hopf bifurcation may lead to incredibly complex phenomena (Gambaudo [1985]). Plaut and Hsieh (Plaut and Hsieh [1987]) studied a one-DOF mechanical system with delay and excitation and found periodic, chaotic and unbounded responses. Forcing of a Duffing-type equation without delay can also result in complicated bifurcation structure (Sanchez and Nayfeh [1990]; Zavodney et al. [1990]).

REFERENCES

Balachandran, B., Kalmár-Nagy, T., and Gilsinn, D.E. (2009). *Delay differential equations*. Springer.

Casal, A. and Freedman, M. (1980). A Poincaré-Lindstedt approach to bifurcation problems for differential-delay equations. *IEEE Transactions on Automatic Control*, 25(5), 967–973.

Gambaudo, J.M. (1985). Perturbation of a Hopf bifurcation by an external time-periodic forcing. *Journal of differential equations*, 57(2), 172–199.

Hanna, N. and Tobias, S. (1974). A theory of nonlinear regenerative chatter. *ASME Journal of Engineering for Industry*, 96(1974), 247–255.

Kalmár-Nagy, T. (2002). Delay-differential models of cutting tool dynamics with nonlinear and mode-coupling effects. *PhD thesis*.

Kalmár-Nagy, T., Stépán, G., and Moon, F.C. (2001). Subcritical Hopf bifurcation in the delay equation model for machine tool vibrations. *Nonlinear Dynamics*, 26(2), 121–142.

Nayfeh, A., Chin, C., and Pratt, J. (1997). Applications of perturbation methods to tool chatter dynamics. *Dynamics and chaos in manufacturing processes*, 193–213.

Nayfeh, A.H. (2008). Order reduction of retarded nonlinear systems–the method of multiple scales versus center-manifold reduction. *Nonlinear Dynamics*, 51(4), 483–500.

Nayfeh, A.H. and Mook, D.T. (1979). Forced oscillations of systems having a single degree of freedom. *Nonlinear Oscillations*, 161–257.

Oztepe, G.S., Choudhury, S.R., and Bhatt, A. (2015). Multiple scales and energy analysis of coupled Rayleigh-van der Pol oscillators with time-delayed displacement and velocity feedback: Hopf bifurcations and amplitude death. *Far East Journal of Dynamical Systems*, 26(1), 31.

Pakdemirli, M. and Karahan, M.M.F. (2010). A new perturbation solution for systems with strong quadratic and cubic nonlinearities. *Mathematical Methods in the Applied Sciences*, 33(6), 704–712.

Plaut, R. and Hsieh, J.C. (1987). Chaos in a mechanism with time delays under parametric and external excitation. *Journal of Sound and Vibration*, 114(1), 73–90.

Sanchez, N.E. and Nayfeh, A.H. (1990). Prediction of bifurcations in a parametrically excited Duffing oscillator. *International Journal of Non-Linear Mechanics*, 25(2-3), 163–176.

Stépán, G. (1989). *Retarded dynamical systems: stability and characteristic functions.* Longman Scientific & Technical.

Zavodney, L.D., Nayfeh, A., and Sanchez, N. (1990). Bifurcations and chaos in parametrically excited single-degree-of-freedom systems. *Nonlinear Dynamics*, 1(1), 1–21.